Available online at www.easdprocedia.org
EASD Procedia EURODYN (2020) 4777-4798

EASD Procedia

EURODYN 2020
XI International Conference on Structural Dynamics
M. Papadrakakis, M. Fragiadakis, C. Papadimitriou (eds.)
Athens, Greece, 23–26 November 2020

MODAL PROPERTIES OF A FLOOR WITH SINGLE-LEAF PLYWOOD ON TIMBER JOISTS: EXPERIMENTAL AND NUMERICAL MODELLING

Lars V. Andersen[1], **Nina Jørgensen**[1], **Gitte S. Iversen**[1] **and Jannick B. Hansen**[2]

[1] Department of Engineering, Aarhus University
Inge Lehmanns Gade 10, DK-8000 Aarhus C, Denmark
e-mail: lva@eng.au.dk

[2] Aarhus School of Engineering, Aarhus University
Inge Lehmanns Gade 10, DK-8000 Aarhus C, Denmark
e-mail: jbah@ase.au.dk

Keywords: Wood, Timber, Floor, Vibration, Modal Analysis, Model Calibration.

Abstract. *The paper addresses the modal properties of a wooden floor consisting of a plywood board fastened by screws to timber joists. The overall aim of the study has been to examine how well finite-element models can be calibrated to match the dynamic properties of a mock-up, studied in the laboratory in a scale of 1:2. The paper proposes the use of output-only modal analysis, also known as operational modal analysis (OMA), using brushes of various stiffnesses to excite the floor. In order to avoid uncertainties related to the supports, free–free boundary conditions are considered. This has been modelled experimentally by suspending the test specimens in rubber bands. Modes up to about 500 Hz were extracted, using an array of accelerometers, and the experimental results were then used as a basis for model calibration and model validation. Two overall approaches to finite-element modelling of the wooden floor are studied in the paper. The first approach employs a solid model with all parts of the structure (plywood and joists) modelled as orthotropic, linear elastic materials. The second approach considers a structural model with the plywood leaf modelled as a laminate shell using Mindlin thick-plate theory and the joists modelled using Timoshenko beam theory. Firstly, the finite-element models of each individual component of the floor, i.e. each beam or plate, are updated with the use of the measured modal properties. Secondly, in order to validate the finite-element models of the assembled floor, their modal properties are compared with the results obtained experimentally. In the validation step, no further updating is performed, but various configurations of the connections between the wooden beams and the plywood board are included in the study. An artificial elastic layer and modelling of the individual lines of screws are introduced within the solid model to allow more realistic modelling of the connection. In this context, the kinematic constraints enforced within the shell–beam model are discussed.*

ISSN:2311-9020
Peer-review under responsibility of the Organizing Committee of EURODYN 2020.
doi: 10.47964/1120.9388.20288

1 INTRODUCTION

Vibrations in a floor can be caused by walking on the floor as well as other sources inside or outside a building. At low frequencies from 1–80 Hz, this can be felt as whole-body vibrations or heard, for example, as rattling noise. In the frequency range 20–250 Hz, the structure-borne vibrations lead to reradiated noise. The noise and vibration may cause annoyance to the inhabitants of a building and, in severe cases, health problems [1–3].

The vibrations of a floor and the related reradiated structure-borne noise are greatly influenced by the modal properties of the floor. These properties are subject to large uncertainties due to natural variations in the material [4,5] and the usage of the floor [6–9] as well as the support conditions and internal joints [10,11]. This entails detailed information about the individual floor if a reliable computational model of the floor is to be constructed. Without such knowledge, the error in the estimate of the natural frequency of a floor may exceed 20 %.

Before a computational model based on, for example, the finite-element (FE) method can be calibrated to match the modal properties identified from measured accelerations, the model must first be able to represent the dynamic response in the frequency range of interest. This paper concerns the frequency ranges relevant to whole-body vibration and reradiated structure-borne noise. For low vibration levels at these frequencies, reinforced concrete floors may be modelled as shells with isotropic, linear elastic material behaviour of the concrete, accounting for the steel reinforcement as layers with additional stiffness in the direction of the rebar. However, a similarly simple approach cannot be used for wooden floors. Timber is an orthotropic material, and the position and orientation of each joist or layer in a plywood laminate must be accounted for explicitly. Furthermore, the uncertainties of the material properties as well as the internal joints between the beams and the plates must be addressed.

The purpose of the paper is to analyse whether FE models based on different overall concepts can be used to model the dynamic behaviour of a wooden floor consisting of a single-leaf plywood board attached to four timber beams by screws in different configurations. Free–free conditions and an empty floor have been considered to avoid additional uncertainties related to the supports and usage of the floor. An experimental campaign has been conducted with the aim of extracting the modal parameters of a mock-up built in scale 1:2. The modal properties of the individual components, i.e. the timber beams and the plywood board, have also been determined experimentally to allow a stepwise model updating. Usually, the modal properties would be obtained by experimental modal analysis (EMA) [12–15], but this paper proposes the use of output-only modal analysis—or operational modal analysis (OMA)—as an alternative to this [16,17], applying diffuse white-noise excitation with soft and medium-stiff brushes.

Two FE modelling concepts are considered: a) a solid FE model and b) a structural FE model. The models are compared regarding their ability to represent the modal properties of the individual components before validating the FE models of the assembled floor with various configurations of the connections.

The overall geometry, connectivity and material properties of the studied wooden floor are presented in Section 2. Section 3 provides an overview of the experimental campaign. Firstly, the experimental setup and testing procedure for each of the tests are described, and then the results are presented. Next, Section 4 introduces the FE models. The geometry, material modelling, discretization, and assembly strategy are all described with focus on the solid FE models. The calibration and validation of the FE models then follow in Section 5. A sensitivity study is first performed to quantify the importance of each material property in the orthotropic material models. A model updating of each beam and the plate is conducted, before the models of the assembled floors with different configurations of screws are validated. Finally, a short summary, the main conclusions, and suggestions for future work are presented in Section 6.

2 DEFINITION OF THE FLOOR MODEL

Ideally, to examine how well an FE model may replicate the modal properties of a wooden floor structure, the FE model should be compared to and validated by a physical floor model in full scale. However, a full-scale model of a floor requires a considerable amount of space and time to build in a laboratory. Further, as the experimental campaign was conducted in the Dynamics Laboratory of Aarhus University School of Engineering, the mock-up of the floor panel should fit into the available test stand. Hence, it was chosen to construct the mock-up in smaller scale, approximately 1:2 compared to a full-size floor. While this allowed easier handling of the timber beams and the plywood plates constituting the floor panel, it still provided an experimental model representative of the kinematic and dynamic behaviour that can be expected for a full-size floor. The geometry and dimensions of the down-scaled model are shown in Figure 1. All beams (*Södra reglar*) came from the same badge in order to get insight into the variation in material properties that can be expected even in that case. Also, two plywood boards (*Keflico Selex Radiata Pine Krydsfiner*) from the same badge were tested to examine the variation in material properties before the modelling of the assembled floor panel.

Prior to conducting the tests and setting up the FE models, it was necessary to have an initial idea of the material properties as well as their upper and lower bounds to be used in the model updating and calibration process. With the initial values, FE analysis and simple hand calculations could be carried out for the beams as well as the boards in order to get insight into the eigenfrequencies and the related eigenmodes, such that the sampling frequency, recording time, and the position of accelerometers used for measurements could be chosen on an informed basis. The upper and lower bounds could be used in the FE model updating (calibration) procedure.

Tables 1–2 show the material properties of the timber beams, based on two different overall assumptions. Thus, for the beams, two sets of parameters are given assuming that the wood is either isotropic (Table 1) or orthotropic (Table 2). In any case, the material is assumed to

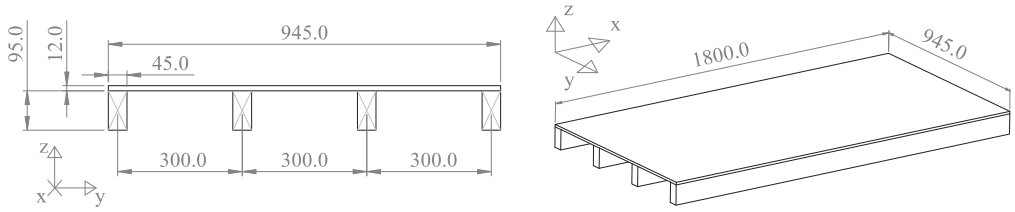

Figure 1: Down-scaled panel section (measures in mm).

	Young's modulus [MPa] E	Poisson's ratio [-] ν
Lower limit	5 600	0.10
Upper limit	17 000	0.49
Initial value	12 440	0.334

Table 1: Isotropic material properties for the beams. Mass density: $\rho = 450$ kg/m^3.

	Young's modulus [MPa]			Shear modulus [MPa]			Poisson's ratio [-]		
	E_1	E_2	E_3	G_{12}	G_{13}	G_{23}	ν_{12}	ν_{13}	ν_{23}
Lower limit	5 600	230	230	440	440	21	0.34	0.34	0.20
Upper limit	17 000	1 200	1 200	1 600	1 600	125	0.72	0.72	0.60
Initial value	12 440	812	812	1 136	1 136	83.4	0.568	0.568	0.44

Table 2: Orthotropic material properties for the beams. Mass density: $\rho = 450$ kg/m^3.

	Young's modulus [MPa]			Shear modulus [MPa]			Poisson's ratio [–]		
	E_1	E_2	E_3	G_{12}	G_{13}	G_{23}	v_{12}	v_{13}	v_{23}
Lower limit	5 860	3 220	1 005	290	61.5	20.5	-0.108	0.156	0.116
Upper limit	12 460	9 820	1 505	940	211.5	170.5	0.142	0.656	0.616
Initial value	9 820	7 180	1 305	680	151.5	110.5	0.042	0.456	0.416

Table 3: Orthotropic material properties for the plywood *single-layer plate*. Mass density: ρ = 500 kg/m^3.

	Young's modulus [MPa]			Shear modulus [MPa]			Poisson's ratio [–]		
	E_1	E_2	E_3	G_{12}	G_{13}	G_{23}	v_{12}	v_{13}	v_{23}
Lower limit	8 200	270	560	350	590	33	0.21	0.12	0.01
Upper limit	21 700	770	1 460	900	1 540	88	0.71	0.62	0.51
Initial value	16 300	570	1 100	680	1 160	66	0.51	0.42	0.31

Table 4: Orthotropic material properties for the plywood *lamina*. Mass density: ρ = 500 kg/m^3.

undergo linear elastic deformation given the very low excitation levels associated with the experiment. It should be noted here that wood is behaving as an orthotropic material. Modelling the wood as isotropic will overestimate the shear moduli as well as the Young's moduli in the directions orthogonal to the grain. The intervals for the values are chosen based on the previous study by Flodén et al. [14], and the initial values are a qualified guess based on the mass density that has been provided by the supplier.

Next, Tables 3–4 show the material properties for the plywood boards in terms of lower and upper bounds as well as the assumed initial values. Here, it was judged that an isotropic material behaviour would be inappropriate, even for the first few eigenmodes. Instead, two alternatives based on orthotropic behaviour were considered: a "smeared-out model" with a single-layer plate (Table 3) and a model with five plies, or laminae, with identical properties by having different orientation of the grain (Table 4). Here, the material properties were inspired by the work on Scots Pine carried out by Gerrand [18]. It is noted that, for the individual lamina, E_1 is the Young's modulus in the grain direction while E_2 is the Young's modulus in the transverse direction parallel to the annual rings. In the single-layer plate model, E_1 is the Young's modulus in direction 1 in which most of the laminae have the grain direction, and E_2 is then the in-plane direction orthogonal to direction 1. The difference between E_1 and E_2 is assumed to be small, since three laminae are present in direction 1, whereas two laminae are present in direction 2.

In addition to the material properties, the assembly between the individual parts of the floor must also be modelled correctly in an FE model. In the present analyses, the plywood board was attached to the beams by screws of the brand Carl Ras (Panel Twistec Ruspert with Fibercut Point no. 4848-0653). The screws had the length 40 mm, and the head had a diameter of 4.0 mm. A total of six configurations were considered for the assembly:

- Panel A: One line of screws per beam, c–c distance of screws: 191 mm
- Panel B: One line of screws per beam, c–c distance of screws: 95.5 mm
- Panel C: One line of screws per beam, c–c distance of screws: 47.8 mm
- Panel D: Three lines of screws per beam, c–c distance of screws: 191 mm
- Panel E: Three lines of screws per beam, c–c distance of screws: 95.5 mm
- Panel F: Three lines of screws per beam, c–c distance of screws: 47.8 mm.

At the ends of the beams, the screws were placed 40 mm from the edges.

Figure 2 shows the overall placement of the screws in Panel A. Further, in the lower–right corner of the figure, an encircled area can be found, indicated by the letter A. This refers to

Figure 3 which provides an overview of the screw positions in all six cases, i.e. Panels A–F. As described below, a part of the research has focused on testing whether a single screw present in the width direction of each beam (Panels A–C) provide a line coupling. Also, it has been examined whether three screws present across the beams (Panels D–F) provide a rigid coupling such that the beams can be considered fully merged with the board.

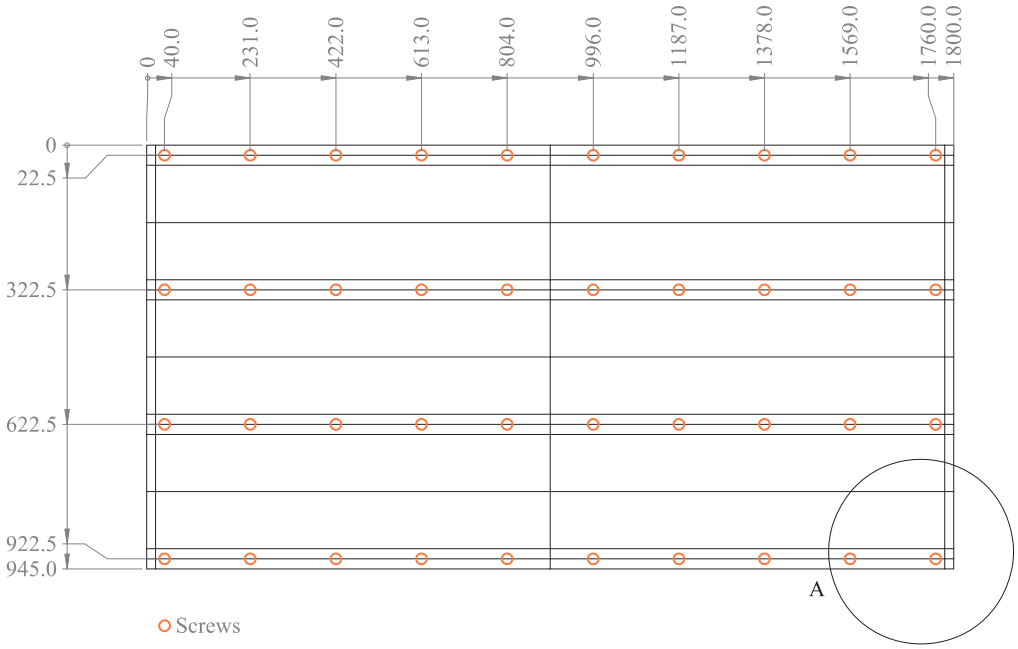

Figure 2: Top view of the floor model with placement of the screws in Panel A.

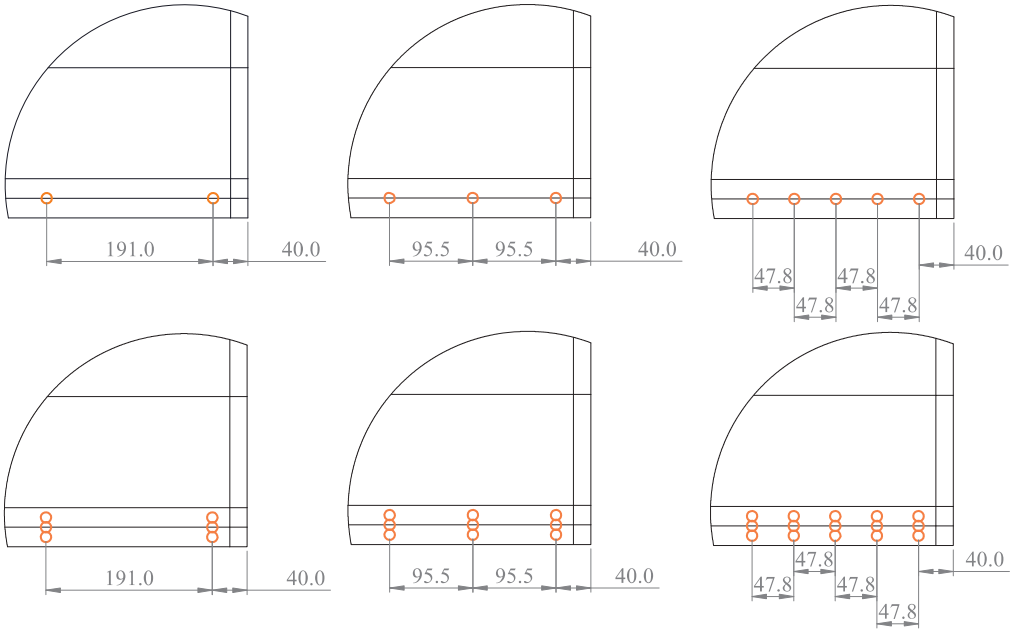

Figure 3: Position of the screws within the encircled area indicated in Figure 2. Top row, left to right: Panel A, Panel B, and Panel C; bottom row, left to right: Panel D, Panel E, and Panel F.

3 EXPERIMENTAL SETUP AND TESTING

The overall purpose of the experimental campaign was to collect reliable data that could be used for the validation and calibration of the FE models. For real floors, constituting a part of a building, uncertainties are associated not only with the material properties but also the support conditions and the usage of the floor, as discussed, for example, by Andersen and co-workers [7–10]. In order to minimize the possible influence of such uncertainties, an empty floor was considered, and so-called free–free conditions (i.e. an unsupported floor) were assumed. In practice, this was established by suspending the test specimens in rubber bands tied at one end to the test rig. Following the procedure suggested by Dickow [19], the other end of the rubber bands was tied by a knot to the eyebolts installed in the test specimens (see Figures 6, 8 and 10). This provides well-defined connections with no sliding or uncertain mechanisms involved.

The experiments were carried out as Output Only Modal Analysis (OMA) [16], using brushes to excite the test specimens. To allow a stepwise calibration of the FE model, updating the material properties of the beams and the boards before analysing the assembled floor, the experimental campaign was conducted in three main steps:

- OMA of the four timber beams, one at a time, conducting four tests for each beam (see Subsection 3.1)
- OMA of the two plywood boards, one at a time, conducting four tests for each board (see Subsection 3.2)
- OMA of the assembled floor, using Board no. 2 and Beams no. 1–4, conducting three to four tests for each of the six panel configurations (see Subsection 3.3).

The specimens were not dismounted between the different tests. For the OMA of the individual beams and boards, a soft brush was utilized for excitation, and for the assembled floor, the same brush as well as a medium soft brush were applied to excite a wider range of frequencies.

The data collection was performed with sensors from Brüel & Kjær (B&K) and a data acquisition system National Instruments (NI):

- 20 pcs. B&K Type 4508-B-002, Piezoelectric CCLD Accelerometer, 1000 mV/ms^{-2}
- 1 pc. B&K Type 4508-B, Piezoelectric CCLD Accelerometer, 100 mV/ms^{-2}
- B&K Type UA-1407, Plastic Mounting Clips
- B&K Type 4294, Accelerometer Calibrator, hand-held
- NI Type cDAQ-9178, CompactDAQ Chassis
- 5 pcs. NI Type 9234, C Series Sound and Vibration Input Module
- Stanley 0-77-030 Moisture Meter
- TinyTag Type TGP-4500, Temperature and Relative Humidity Logger.

Furthermore, a level was used to make sure that the various specimens were mounted in a horizontal position, and a scale was used to determine the weights.

The experimental data were recorded using NI SignalExpress [20] with DAQ Assistant [21] installed. Analyses were carried out using ARTeMIS Modal Pro [22], and a quick pre-analysis of the recorded data was performed in MATLAB [23] using the OMA Toolbox [16] to see whether reasonable eigenfrequencies modes were obtained. In the instrumentation of the specimens, care was made to place accelerometers such that global as well as local modes of vibration would be registered. For the assembled floor, accelerometers should therefore not be placed only on top of the beams, but also on the boards in the mid-spans between the beams. Examples of global bending and local vibration modes for the assembled floor can be seen in Figure 4.

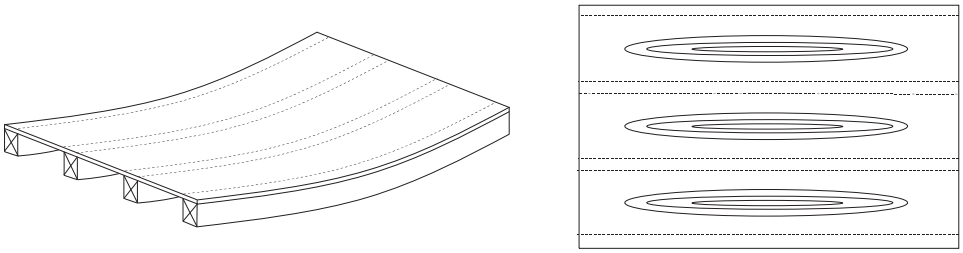

Figure 4: Example eigenmodes of panel: Global bending (left); local plate deflection between joists (right).

3.1 Output-only modal analysis of the individual beams

Figure 5 shows the position of the accelerometers mounted on each single beam in the first step of the experimental campaign. Further, Figure 6 shows the experimental setup with one of the beams mounted in the test rig. Nine accelerometers were placed on the top flange of the beam and another nine accelerometers were placed on one side. No accelerometers were placed on the bottom flange or on the other side, since no modes with significant deformation of the cross-section were expected within the considered frequency range. All wires were carefully attached to a wooden rod placed above the beam to avoid any collisions with the beam during the experiment. Each test lasted 30 s, and the data was acquired at a sampling frequency of 2 049.2 Hz. The soft brush was applied for excitation.

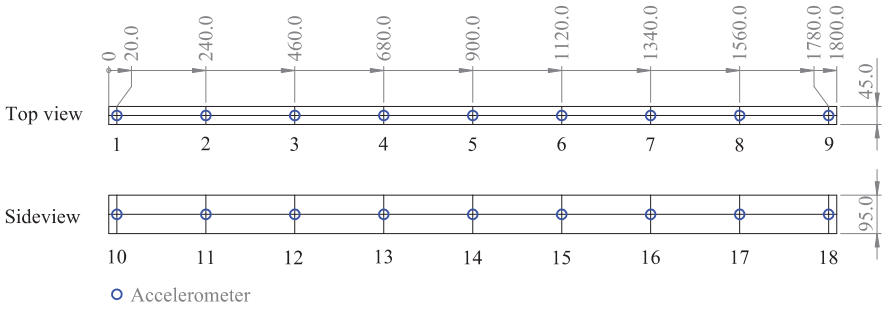

Figure 5: Position of the accelerometers mounted on each single beam.

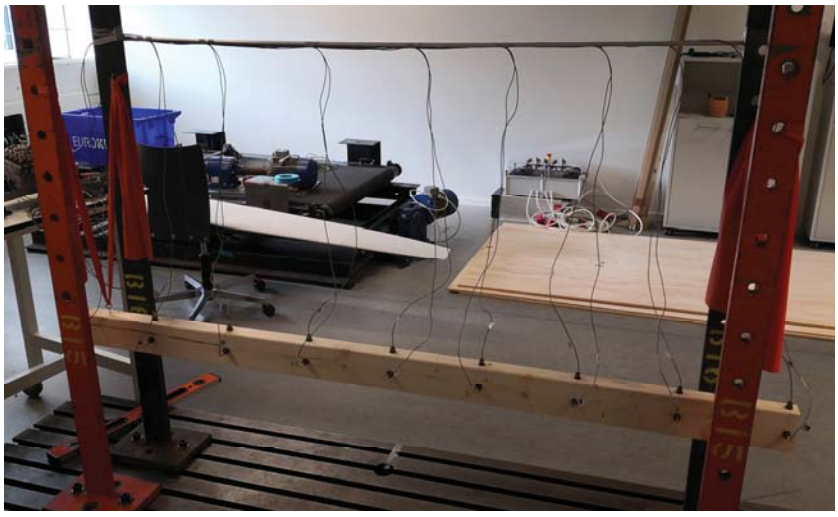

Figure 6: One of the wooden beams placed in the test stand.

3.2 Output-only modal analysis of the board

Figure 7 shows the positions of the eyebolts and the accelerometers mounted on each single plywood board. Figure 8 illustrates the experimental setup with one of the boards mounted in the test rig. It should be noted that Figure 7 indicates the positions at which the beams were later placed (the sides as well as the centre lines of the beams). The accelerometer positions were carefully chosen to capture as many modes as possible within the considered frequency range. Also, the eyebolts were placed at the positions where preliminary analyses based on the initial material properties in Table 4 indicated a small deflection in the first eight eigenmodes. Each test lasted 120 s, and the sampling frequency was set to 1 652.9 Hz. The soft brush was applied for excitation.

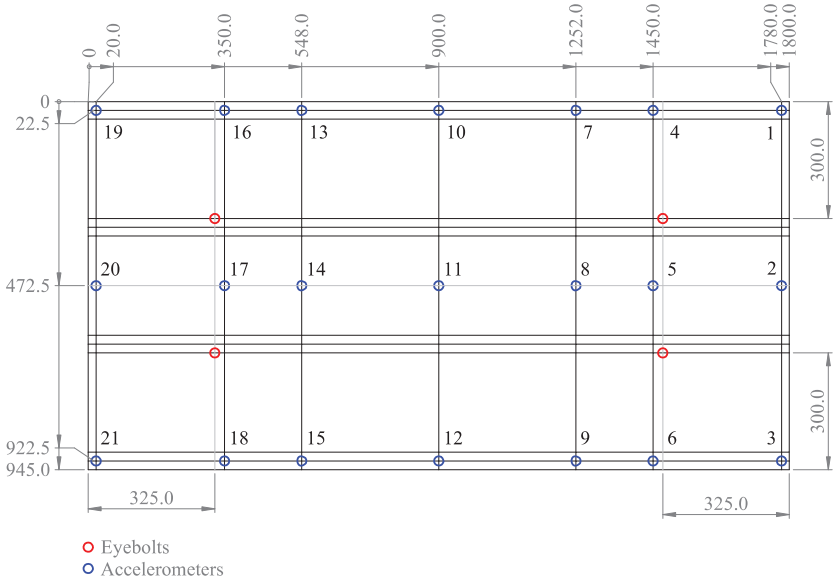

Figure 7: Position of the accelerometers on each of the plywood boards (top view).

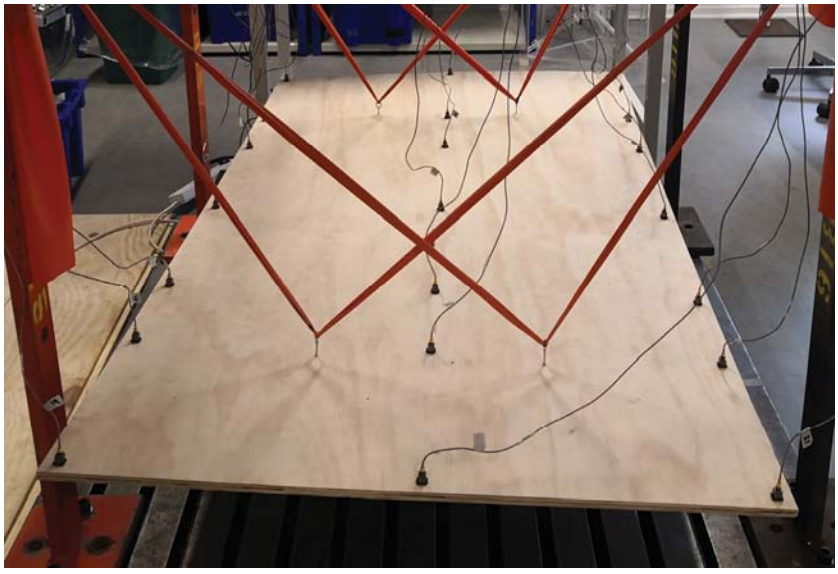

Figure 8: One of the plywood boards placed in the test stand.

3.3 Output-only modal analysis of the complete floor panel

The positions of the accelerometers and the eyebolts mounted on the assembled floor panel are shown in Figure 9. Again, the positions have carefully been selected based on a preliminary FE analysis using the initial material properties for the timber beams (Table 2) and the plywood

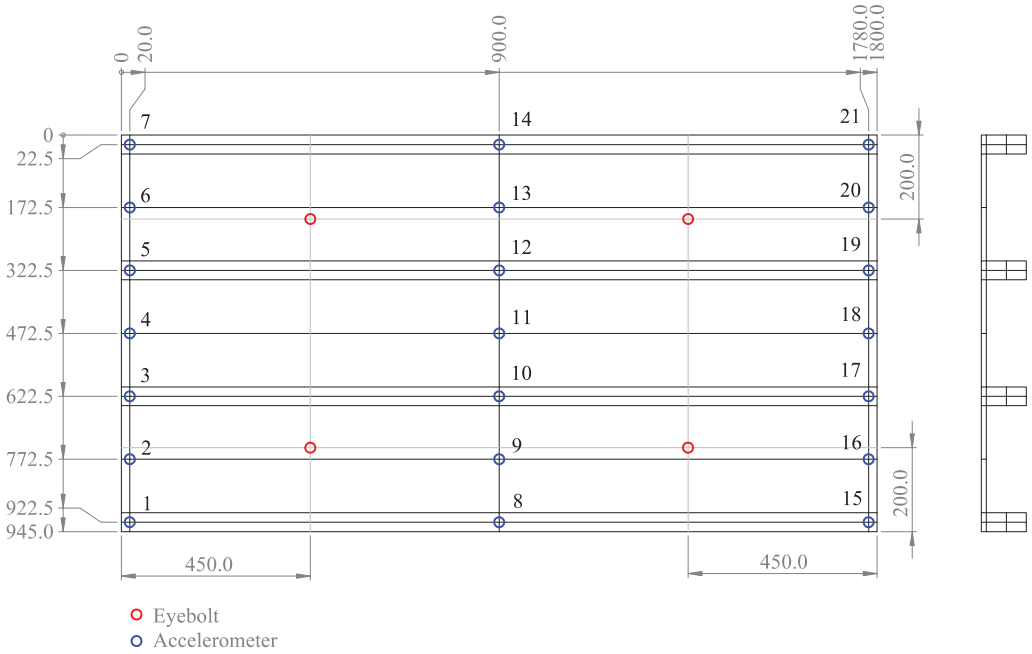

Figure 9: Position of the accelerometers on the assembled floor (top view).

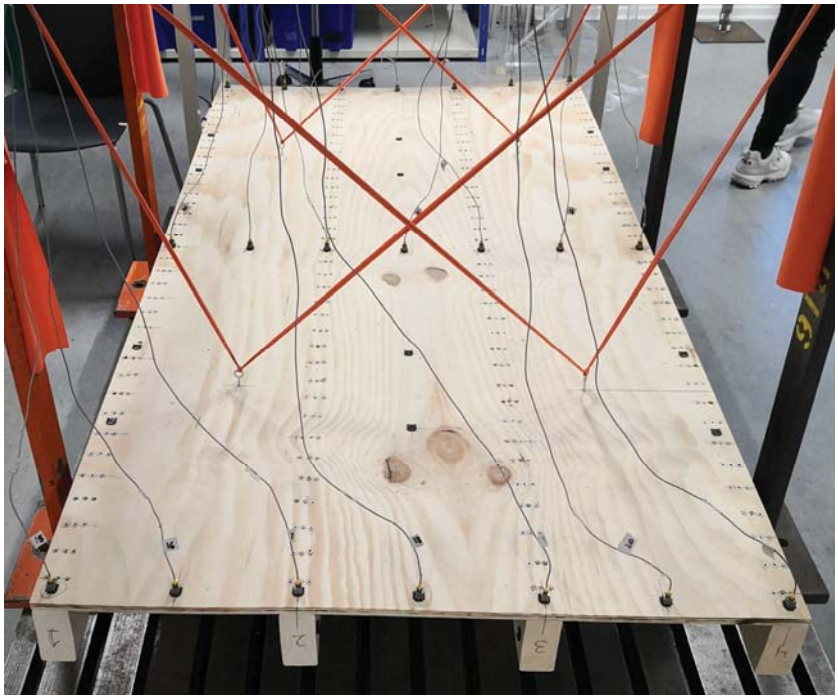

Figure 10: The mock-up of the floor (Panel F) mounted in the test rig.

board (Table 4). Figure 10 shows the setup with the assembled floor panel installed in the test rig. The photograph illustrates Panel F, i.e. the configuration with three screws over the width of each beam and with 47.8 mm between the screws in the longitudinal direction. Among the considered panel configurations, this is the most rigid connection between the beams and the board. Each test lasted 45 s, and the sampling frequency was set to 1 652.9 Hz. The soft and medium soft brushes were applied for excitation.

3.4 Results of the experimental campaign

The mass densities of the individual beams were found to be 415.32, 539.19, 444.31, and 442.85 kg/m^3, for Beams 1, 2, 3, and 4, respectively. Thus, Beam 2 had a relatively high mass density compared to the other beams, even though all beams came from the same badge. The mass densities of the boards were 490.09 and 483.25 kg/m^3, for Plates 1 and 2, respectively.

A full report of the experimental results is beyond the scope of the paper. However, information about the mean values of the eigenfrequencies extracted for each of the components as well as for the assembled floor are given in Tables 5–7. The first eigenfrequency of the beams is related to bending in the horizontal plane, i.e. with respect to the weak axis of the cross section, and it lies close to 70 Hz. Mode 2 relates to bending in the vertical plane, i.e. with respect to the strong axis. As expected, the corresponding eigenfrequency is approximately twice as high as the eigenfrequency related to Mode 1. It is furthermore interesting to note that Modes 4 and 7 are the first and second torsional modes according to the finite-element models. Given the instrumentation of the beams, these modes were not captured in the OMA. This explains that these modes are missing in Table 5.

The plates (plywood boards) were much more flexible than the beams. Here, the first ten eigenmodes had frequencies in the interval from around 10 Hz to approximately 80 Hz. With the chosen position of the accelerometers, all the first ten modes could be captured by OMA. It is noted that the first mode at around 10–12 Hz relates to torsion, whereas the second mode relates to bending of the plates. Except for Modes 4 and 5, Plate 1 had a stiffer response than Plate 2, i.e. the extracted eigenfrequencies for Plate 1 are higher than those for Plate 2.

Finally, Table 7 shows that the eigenfrequencies related to the first ten modes of the assembled floor panels lie in the range 15 Hz to 200 Hz. By comparison with FE models of the six panels, it was identified that Mode 2 of Panel B was not captured by the OMA. The same problem occurred for Modes 1 and 2 of Panel D. Interestingly, the eigenfrequencies related to some of the modes, e.g. Modes 1, 4, 5 and 10, are close to being identical for the various configurations of the screws. For Mode 10, only Panel A with the smallest amount of screws has a significantly lower eigenfrequency than the other configurations. However, for some of the modes, e.g. Modes 7 and 9, there is a marked difference between the panels with few or many screws. The number of screws in the longitudinal direction and the number of screws across each beam are equally important. It should in this context be mentioned that the first eight eigenmodes of the full panel do not involve bending of the beams which are relatively stiff.

Further, the relative variations in the extracted eigenfrequencies of all specimens are shown in Figure 11. For a given eigenmode of the beams it can be observed that the associated eigenfrequencies of the individual beams differed up to about 5 percent from the mean value based on all four beams. As also seen in Table 5, Beam 2 provided consistently higher eigenfrequencies than the other beams for the first four modes. The higher mass density of Beam 2 is therefore associated with an even higher stiffness. For the plates, some variation also occurs, and it can be observed that none of the boards provides frequencies that are consistently higher than the other board. This indicates that the eigenfrequencies are very sensitive to variations of the material properties in the different laminae and in different directions or planes.

	Beam 1	Beam 2	Beam 3	Beam 4
Mode 1	69.04	73.67	68.91	68.54
Mode 2	144.75	147.34	142.83	145.08
Mode 3	187.77	195.86	180.73	191.28
Mode 4 (5)	351.54	376.22	367.59	358.37
Mode 5 (6)	372.88	360.58	354.83	382.39
Mode 6 (8)	573.50	590.22	558.82	570.83
Mode 7 (9)	650.37	660.26	682.02	673.72
Mode 8 (10)	831.65	836.11	795.96	805.30

Table 5: Average eigenfrequencies (Hz) for the beams based on four OMA tests on each beam. The mode numbers given in parenthesis refer to the mode numbers obtained by the finite-element models.

	Plate 1	Plate 2
Mode 1	12.26	10.49
Mode 2	15.06	14.63
Mode 3	27.41	25.73
Mode 4	32.27	33.23
Mode 5	35.79	36.59
Mode 6	42.84	41.16
Mode 7	52.74	49.97
Mode 8	54.07	53.30
Mode 9	77.83	75.19
Mode 10	80.59	78.42

Table 6: Average eigenfrequencies (Hz) for the plates based on four OMA tests on each plate.

	Panel A	Panel B	Panel C	Panel D	Panel E	Panel F
Mode 1	15.64	15.69	15.54		15.50	15.57
Mode 2	13.94		16.01		16.51	16.75
Mode 3	32.08	34.26	35.55	34.84	36.05	36.35
Mode 4	41.93	42.19	42.24	42.14	42.24	42.37
Mode 5	56.26	58.11	59.19	58.65	59.62	59.99
Mode 6	81.48	85.73	87.30	86.49	88.48	89.35
Mode 7	105.12	115.50	119.72	116.93	122.20	124.36
Mode 8	139.69	142.67	143.02	142.01	142.79	143.12
Mode 9	161.82	168.45	172.41	170.73	174.93	175.91
Mode 10	191.32	198.41	200.79	197.23	200.29	200.42

Table 7: Average eigenfrequencies (Hz) for the panels based on three to four OMA tests on each panel.

Figure 11 shows that some of the panel configurations provide eigenfrequencies that are significantly lower than other configurations. Especially, in eigenmode 2, Panel A (which has the smallest amount of screws) provides an eigenfrequency that is about 20 percent lower than that of Panel F (which has the largest amount of screws). This clearly demonstrates that the connectivity between the beams and the plate has a large impact on the modal properties of the floor, even for the first eigenmodes. It should again be noted that Mode 2 of Panel B and Modes 1 and 2 of Panel D were not captured during the experiments.

Finally, Figure 11 shows that there was a small scatter in the repeated recordings for the individual structural members as well as the floor panels. Part of this variation can be attributed to the changing environmental conditions caused, primarily, by an irregularity in the operation

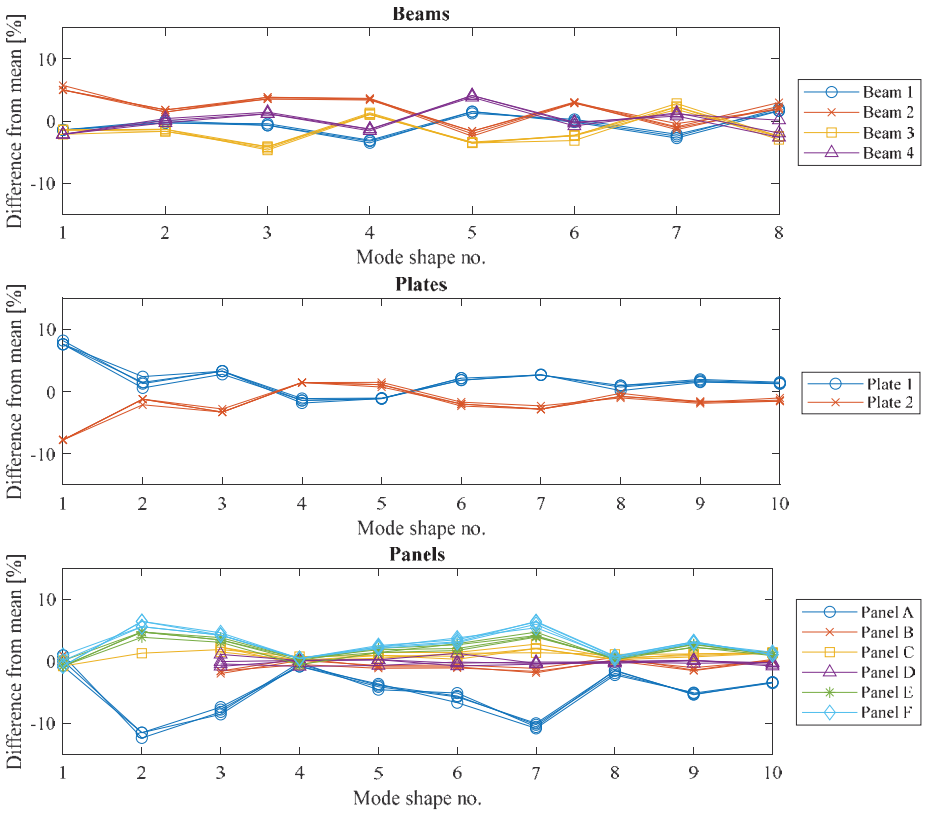

Figure 11: Relative variations in the experimentally measured eigenfrequencies.

of the ventilation system in the laboratory. During the experimental campaign, the temperature varied between 20.2 °C and 22.6 °C, and the relative humidity varied between 28.6 % and 50.3 %. It was observed that one of the plywood boards, Plate 1, warped because of a change in moisture content, and for this reason, only Plate 2 was used for the floor assembly.

4 FINITE-ELEMENT ANALYSIS OF THE WOODEN FLOOR PANEL

The finite-element modelling process followed the same steps as the experimental campaign in order to allow a direct comparison, validation and calibration of the FE models. Thus, as a first step, the individual beams and plates were modelled. Two overall concepts were applied: a three-dimensional (3D) solid FE model of each part developed in Abaqus, and a 3D structural FE model developed of each individual part developed in MATLAB.

The MATLAB model of the beam was based on two-node Timoshenko beam elements using the standard cubic Hermite interpolation functions. Linear interpolation was used for the axial and torsional deformations, assuming Saint-Venant torsion. Since the beam theory assumes that cross sections remain undeformed, only E_1, G_{12} and G_{13} influence the stiffness when utilizing an orthotropic material model. It is noted that the torsional stiffness depends on a combination of G_{12} and G_{13}, whereas transverse shear depends on either G_{12} or G_{13}, depending on direction.

For the plywood boards, the MATLAB model employed Mindlin thick-plate theory. Nine-node elements with quadratic Lagrange interpolation of the displacements and rotations were utilized. Selective integration was applied for the in-plane directions of the element to avoid locking, and a three-point Gauss quadrature rule was applied over the thickness of each ply. The model allows the introduction of a laminate composite with orthotropic behaviour of each

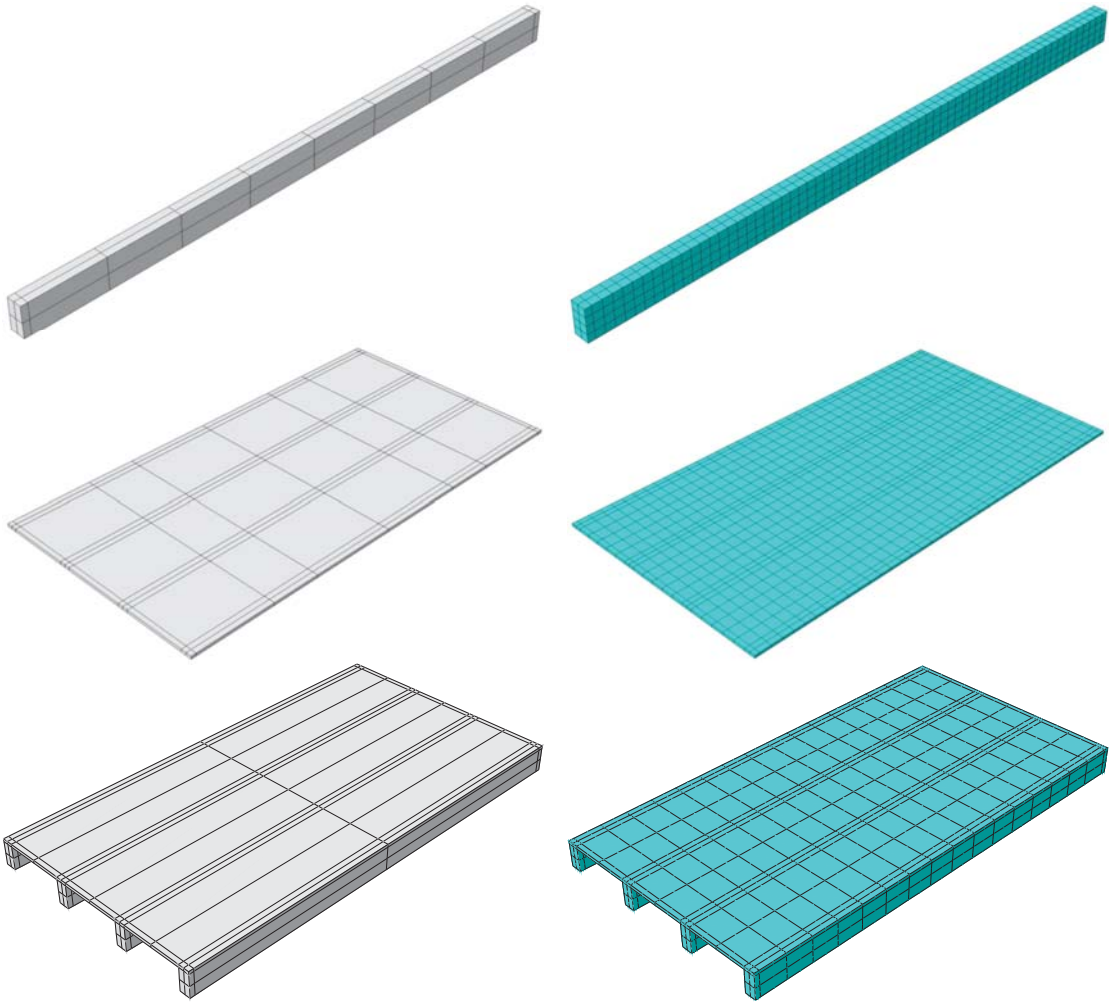

Figure 12: Solid finite-element models of a single beam (top), a plate (middle), and a floor panel (bottom). Left: Division of the geometry. Right: Structured mesh with solid cubes.

layer, or ply. A layup with a 0°–90°–0°–90°–0° configuration was implemented, assuming that the thickness of each ply was the same, corresponding to one-fifth of the plate thickness.

The Abaqus solid FE models of a beam and a plate are illustrated in Figure 12 which also shows a model of an assembled floor panel in which the beams are simple merged with the plate. Generally, the divisions of the models were introduced to allow the evaluation of the displacements at the positions where the accelerometers were placed in the experimental tests. The same strategy was used for the beams and plates in MATLAB. It is noted that the accelerometers were not modelled in any of the models. This implies a modelling uncertainty, but the errors related to the modal properties are assumed to be small.

The 3D solid models are based on 20-node iso-parametric brick elements with quadratic Lagrange interpolation of the displacements and full integration. The Abaqus models were implemented via Python scripting to allow easy modification of material properties and geometry. Further, the input files for Abaqus/Standard are directly transferable to FEMtools [24]. As explained in Section 5, this was later used for automatic model updating aimed at identification of the material properties. However, it should be noted that orthotropic material behaviour must be treated with care, because Abaqus and FEMtools order the material properties differently.

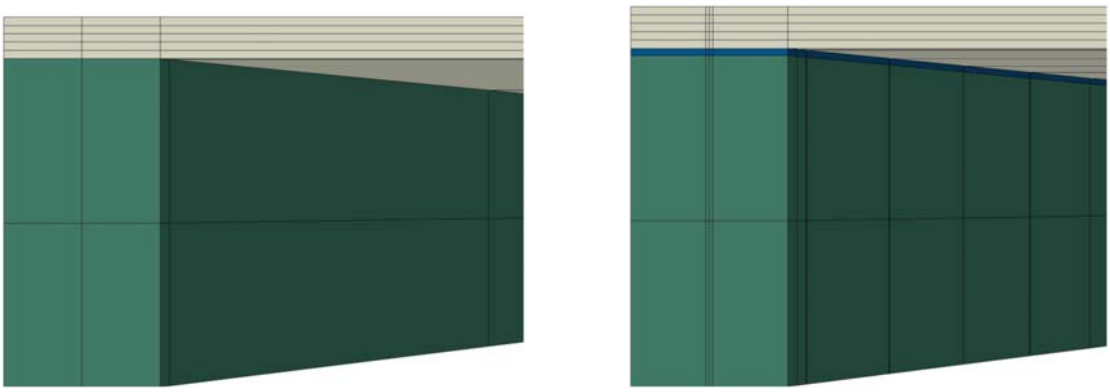

Figure 13: Configurations of the coupling between the beams and the plate in the 3D solid finite-element model. Left: Merged model with direct coupling of the beams to the plate. Right: Coupling via an artificial layer.

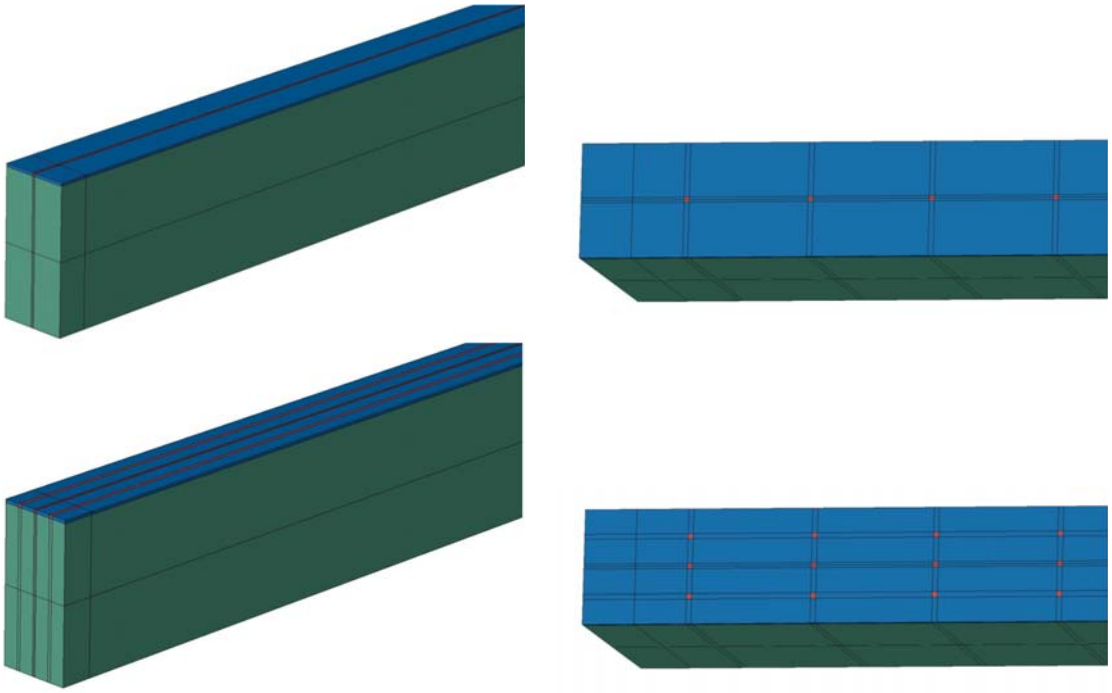

Figure 14: Modelling approaches for the screwed connections between the beams and the plate. "Line" couplings (left) and "point" couplings (right) for a single line of screws (top) or three lines of screws (bottom).

Different approaches to coupling of the beams and the plate were tested in the solid FE model. The simplest configuration merely introduced a full coupling by merging the beams with the plate. To allow a more realistic modelling of the coupling, a 2 mm thick artificial elastic layer was introduced in the remaining models, as illustrated in Figure 13. Based on a previous study by Dickow et al. [25], the layer was assumed to have a mass density of 450 kg/m^3, a Young's modulus of 4 MPa, and a Poisson's ratio of 0.05.

As shown in Figure 14, two strategies were used to model the screws: "line" couplings with 4 mm wide zones resembling the single lines of screws in Panels A–C or the three lines of screws in Panels D–F; "point" couplings with 4 mm × 4 mm zones at the positions of the individual screws. The material in the zones representing the screws was assumes to be steel with the mass density 7 850 kg/m^3, the Young's modulus 210 000 MPa, and the Poisson's ratio 0.30.

5 MODEL CALIBRATION AND UNCERTAINTIES

Based on the experimental tests, reported in Section 3, the FE models of Section 4 were calibrated by updating the material properties. The strategy was to first calibrate the models of the beams and plates separately and then to couple the various parts as suggested in Section 4 without additional modification of the properties. A comparison can then be made of the results obtained using the initial properties (see Tables 1–4) and the optimized values. The properties of the artificial coupling layer were not modified in this process, and as such the comparisons serve as a validation of the material properties and modelling approach for this layer.

Before the model calibration, a preliminary sensitivity study was performed to quantify the importance of each material property. The solid model of each part was employed for this analysis. In the following model calibration, only the material properties with significant influence on the eigenfrequencies were included as variables. This ensured a robust optimization at a relatively low computational cost while still exploiting close to the entire potential for fitting the models to the results of the experimental tests. In any case, the material in each beam, and in each ply of the boards, was assumed to be homogeneous.

For the beam with isotropic material behaviour, the Young's modulus is equally important for all modes, whereas Poisson's ratio only influences modes dominated by shear – since in this case $G = E/(2 + 2\nu)$. However, the isotropic beam models were found to provide a poor match to the test results with no possibility to fit more than the first four to five modes within a reasonable accuracy. Hence, only the orthotropic model was used for further analysis. Here, Figure 15 (left) shows the results of the sensitivity analysis. Clearly, the Young's modulus E_1 in the grain direction has a strong influence on four of the first five modes. Mode 4 is dominated by the shear moduli G_{12} and, especially, G_{13}. It is noted that this is the first torsional mode, which explains the weak dependence on E_1. In any case, none of the remaining six material properties have any significant impact, i.e. only E_1, G_{12} and G_{13} are important for the orthotropic beams.

For the plywood board, Figure 15 (right) shows the results of the sensitivity study. Interestingly, G_{12} is very important for Mode 1, and it also has a strong influence on Modes 3 and 5. Mode 1 is the first torsional mode of the board which lies at a frequency slightly below that of the first bending mode (Mode 2). For Modes 2–5, E_1 has the larger impact on the eigenfrequencies. A weak influence can be seen from E_2, G_{23} and ν_{12}, while the remaining properties have no or extremely little influence. However, it may be expected that G_{12} and G_{13} are important for the eigenfrequencies related to higher modes where shear in bending becomes pronounced.

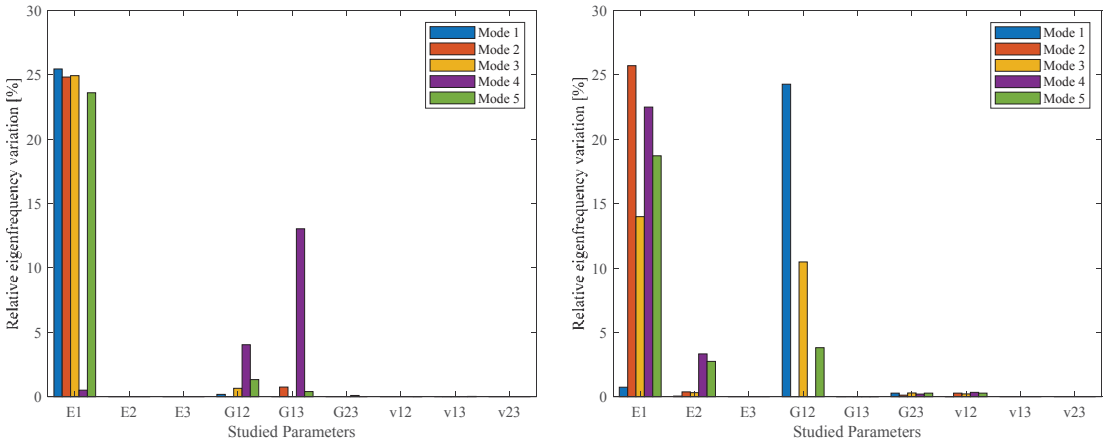

Figure 15: Change in the first five eigenfrequencies due to a variation of each material property by about ±25 % relatively to the initial values suggested for the beams in Table 2 (left) and for the plates in Table 4 (right).

The model updating was performed in FEMtools using, as input, the experimental results from ARTeMIS and the FE models from Abaqus. The initial values as well as the upper and lower bounds for the material properties given in Tables 2 and 4 were used. However, the mass densities found for each specimen using the scales were employed (see Subsection 3.4). As already mentioned, the isotropic beam models will not be analysed further. Likewise, the plate model with a single layer of orthotropic material will not be further regarded in the present analysis, although model updating showed that fair results could be achieved with this type of model for the first few modes of the individual plywood boards.

The model updating was performed based on a comparison of the eigenfrequencies f_i as well as the mode shapes $\{\boldsymbol{\Phi}_i\}$, using the Modal Assurance Criterion (MAC) [26]:

$$\mathrm{MAC}_{ij} = \frac{\left|\left\{\boldsymbol{\Phi}_i^{\mathrm{FE}}\right\}^H \left\{\boldsymbol{\Phi}_j^{\mathrm{EX}}\right\}\right|^2}{\left\{\boldsymbol{\Phi}_i^{\mathrm{FE}}\right\}^H \left\{\boldsymbol{\Phi}_i^{\mathrm{FE}}\right\} \left\{\boldsymbol{\Phi}_j^{\mathrm{EX}}\right\}^H \left\{\boldsymbol{\Phi}_j^{\mathrm{EX}}\right\}}. \tag{1}$$

Here *H* denotes the Hermitian of the vector, the superscripts FE and EX refer to "Finite-Element model" and "Experimental test", respectively, and the indices *i* and *j* refer to Modes *i* and *j*. A MAC value of (nearly) 1 implies that there is (almost) correspondence between the modal vectors for Mode *i* of the FE model and mode *j* of the experiment. This does not guarantee that the modes are (nearly) identical. For example, the related eigenfrequencies may be different, and the response at points that are not included as nodes in the vectors may deviate. On the other hand, if the MAC value is (close to) zero, it can be expected that the modes are inconsistent.

For each structural component, i.e. Beams 1–4 and Plates 1 and 2, the following updating procedure was applied:

- The nodes of the FE model (FE nodes) corresponding to the positions of the accelerometers (experimental nodes) were identified.
- The FE nodes and the experimental nodes were paired in FEMtools.
- The eigenmodes of the FE model and experiment were compared and the modes with MAC values of at least 60 % were included as basis for the model updating.
- A maximum of five iterations were performed to optimize the selected material properties.
- In each iteration, a normalized sensitivity matrix, $[\mathbf{S}]$, was determined, defining the dependence of each observed eigenfrequency on each of the material properties, e.g.,

$$S_{12} = \frac{\partial f_2}{\partial E_1}\frac{E_1}{f_2}. \tag{2}$$

  Here f_2 is the second eigenfrequency of the FE model and E_1 is the value of the Young's modulus in the grain direction of the considered beam or ply based on the previous iteration. See, for example, [17, 18] for further details.
- The change in the material properties was found as $\{\Delta\mathbf{P}\}_{k+1} = [\mathbf{S}]_k^{-1}\left(\left\{\mathbf{f}_k^{\mathrm{EX}}\right\} - \left\{\mathbf{f}_k^{\mathrm{FE}}\right\}\right)$.
- The material properties were updated as $\{\mathbf{P}\}_{k+1} = \{\mathbf{P}\}_k + \{\Delta\mathbf{P}\}_{k+1}$.
- If the difference between the eigenfrequencies of the experiment and the FE model was overall below a given threshold, or if the improvement from one iteration to the next was below a given tolerance, the iteration was terminated even if five iterations had not been reached. The standard values EPS1 = 0.01 and EPS2 = 0.001 were used in FEMtools.

It is noted that the process corresponded to a gradient-based optimization procedure, using a least-squares approach, since there were more eigenfrequencies than material properties.

Table 8 and Figure 16 show the results of the model calibration for the beams. Here, only E_1, G_{12} and G_{13} have been used as variables in the optimization. Compared to the initial values, Young's in the grain direction, E_1, was reduced for Beams 1, 3 and 4, whereas an increase was necessary for Beam 2 in order to provide an optimal fit to the experiment. For all beams, the shear moduli G_{12} and G_{13} were reduced significantly. With reference to Figure 16, the solid FE models developed in Abaqus and the Timoshenko beam FE model implemented in MATLAB provided very similar results for the first seven modes when using the initial values of the material properties. However, the eigenfrequencies deviated about 10 % from the measured values. For Mode 8, there is a large discrepancy between the results of the two FE models. It is noted that this mode occurred at around 800 Hz (see Table 5), i.e. at a very high frequency. After the model updating with the use of FEMtools, a much better fit was obtained. It was thus possible to fit the first eight eigenfrequencies within a relative error of 0–5 %, compared to the experiments for the respective beams. It should be mentioned that an optimization of the MATLAB model was achieved by the introduction of a torsional shear modulus, $G_T = \alpha(G_{12} + G_{13})$. With a proper tuning of the parameter α, a good match of the MATLAB model with the Abaqus model could be obtained, regarding the torsional modes that were not captured experimentally.

Table 9 and Figure 17 show the results of the model updating for the two plywood boards. Poor results were achieved with the initial values of the material properties, but after the model updating with FEMtools, a fair fit was obtained for the first ten modes. It can be observed that the five-layer solid model developed in Abaqus and the Mindlin-shell-element model developed in MATLAB provide similar results both before and after the updating process. Slightly better results were obtained for Plate 2, compared to Plate 1, and as mentioned above, Plate 1 could

Property		Initial value	Beam 1	Beam 2	Beam 3	Beam 4	Average
E_1	(MPa)	12 440	9900	14 256	10 360	10 810	11 332
G_{12}	(MPa)	1 136	635	679	582	531	607
G_{13}	(MPa)	1 136	631	592	815	809	711

Table 8: Model updating of beams with orthotropic material behaviour.

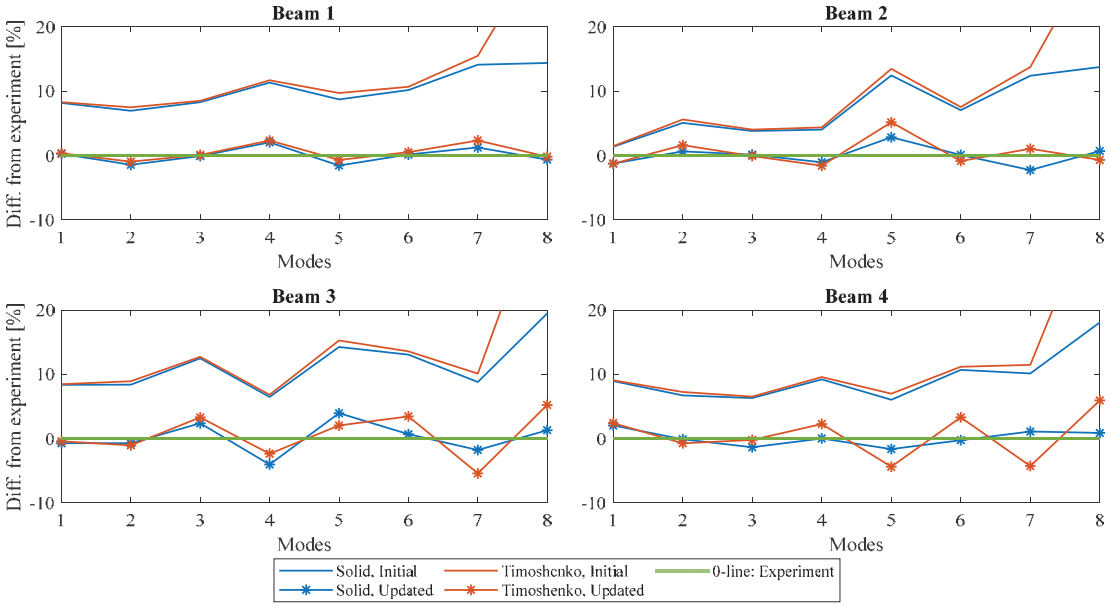

Figure 16: Eigenfrequencies for Modes 1–8 of the beams – deviation from the test results.

		Initial value	Plate 1	Plate 2	Average
E_1	(MPa)	16 300	9 396	8 487	8 942
E_2	(MPa)	570	511	1 031	771
G_{12}	(MPa)	680	1 178	932	1 055

Table 9: Model updating of plywood boards with five-layers of orthotropic material.

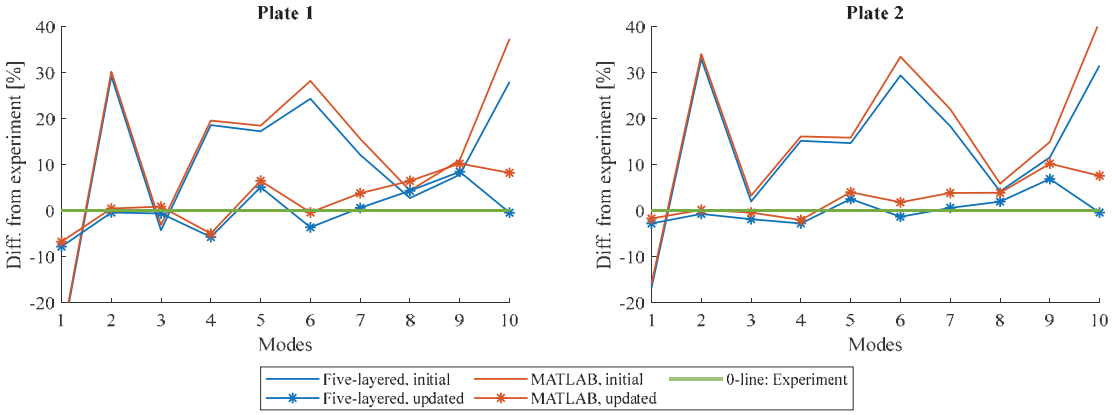

Figure 17: Eigenfrequencies for Modes 1–10 of the plywood boards – deviation from the test results.

not be used in the subsequent assembly of the floor panels, since it was twisted due to uncontrolled variations of the environmental conditions (temperature and humidity) in the laboratory.

Finally, the FE models of the assembled floor panels were compared with the experimental results. Figure 18 shows the results for Panels A–F, based on three different sets of material properties:

- The initial values based on a qualified guess and literature study (see Tables 2 and 4)
- The average updated values of the material properties (see Tables 8 and 9, the last columns)
- The exact updated values of the material properties for each of the structural components (see Tables 8 and 9, the columns for Beams 1–4 and Plate 1).

The deviations from the test results are quantified in terms of the Normalized Relative Frequency Difference (NRFD) [12]:

$$\mathrm{NRFD}_i = \frac{\left| f_i^{\mathrm{FE}} - f_i^{\mathrm{EX}} \right|}{f_i^{\mathrm{EX}}} \cdot 100\ \%\,, \tag{3}$$

where f_i^{FE} and f_i^{EX} are the eigenfrequencies of Mode i obtained by FE modelling and experimental testing, respectively.

The general trend in Figure 18 is that the NRFD is about 30 % for the models employing the initial values of the material properties. For Panel A, the merged FE model provides a very poor result. This was to be expected, given that Panel A has the weakest coupling of the beams and the plate with only a single line of screws for each beam and with almost 200 mm distance between the screws. However, even when modelling the connection between the beams and the plate more realistically, the initial values of the properties lead to erroneous results.

A significant improvement in the accuracy of the FE models was achieved by using the average material properties obtained by model updating. Except for three modes of Panel A, the first ten eigenfrequencies of all the considered panel configurations have an NRFD below 15 % when the beams are merged to the plate within the FE models. When the connections were modelled appropriately, NRFD values below 5 % were obtained with the average values

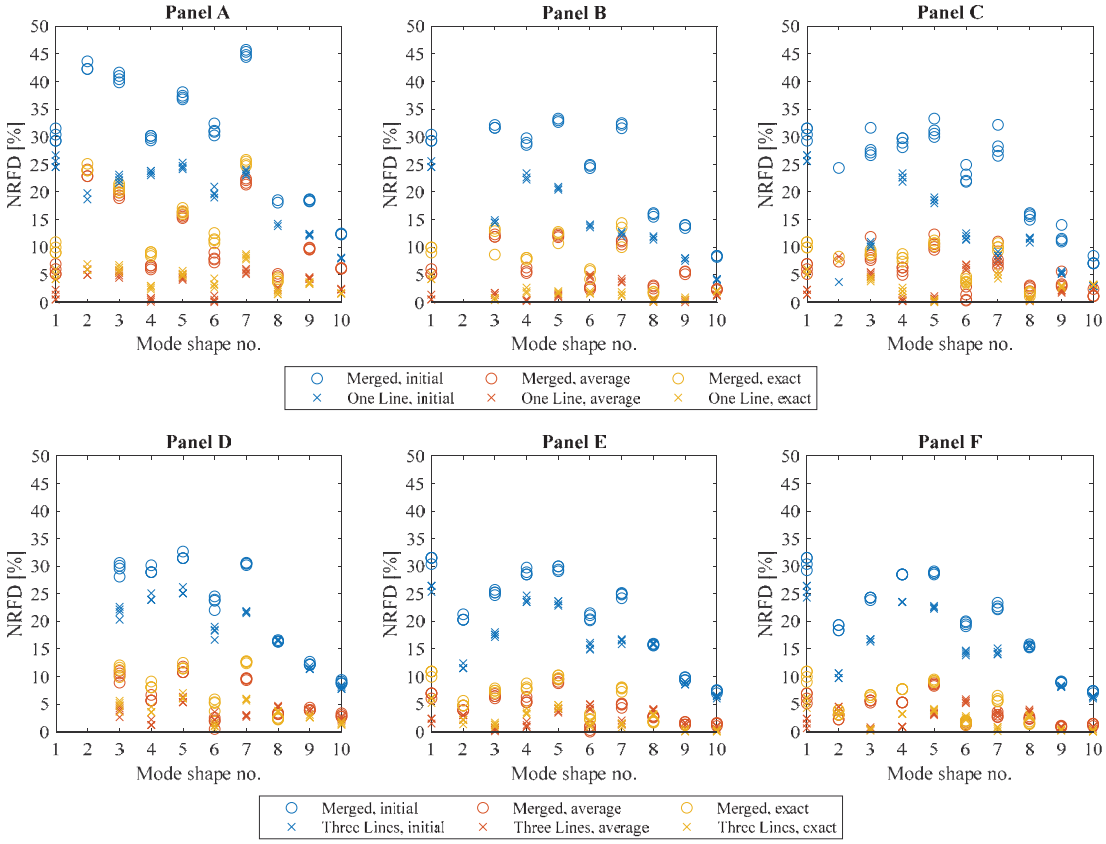

Figure 18: Normalized Relative Frequency Difference (NRFD) plots for the solid FE models of Panels A–F.

of the material properties. Interestingly, no significant improvement could be achieved by using the exact updated values for the individual structural components. For some of the modes, in some of the panels, the average material properties provided the better match, and for the other combinations of modes and panels, the exact updated values resulted in a more accurate fit.

As an alternative to the solid models of the floor panels, a structural FE model based on Timoshenko beam and Mindlin shell elements was implemented in MATLAB. The coupling of the beam and shell elements was introduced in terms of Lagrange multipliers, assuming a rigid link between the nodes of the beams and the nodes of the shell to which they were tied. Kinematically, this introduces a severe constraint, since the beams cannot rotate relative to the shell. Hence, the structural FE model was only able to produce useful results for Panels D–F. For Panels A–C (especially Panels A–B) with the single line of screws coupling each beam to the board, some modes of vibration could not be represented by the MATLAB model.

6 CONCLUSIONS AND SUGGESTIONS FOR FURTHER RESEARCH

A mock-up of a single-leaf floor panel consisting of four timber beams and a plywood board was analysed. An output-only modal analysis (OMA) was conducted for the individual structural components, and it was found that a significant variation in the eigenfrequencies can exist for similar beams coming from the same badge. One of the tested beams was about 25 % heavier than the other beams, and the difference in stiffness was even higher. Hence, some of the eigenfrequencies of the beam with the larger density were higher than the corresponding eigenfrequencies of the other beams.

Three-dimensional finite-element (FE) models were developed in Abaqus and MATLAB, in both cases assuming orthotropic material properties of the wood and modelling the plywood with five layers of the same material. In Abaqus, a solid model was used for the plywood boards and the beams, whereas the MATLAB models were based on structural finite elements employing Timoshenko beam theory and Mindlin plate theory. It was found that only three material properties, E_1, G_{12} and G_{13}, have significant influence on the modal properties of the beams, and only E_1, E_2 and G_{12} are important for the plywood boards.

The results of the experiments and the finite-element models developed in Abaqus were used as input for a model update utilizing the software FEMtools. It was possible to obtain a good match of the first eight eigenfrequencies of the individual beams and the first ten eigenfrequencies of the individual plywood boards within five iterations of the gradient-based updating procedure. Post analysis showed that the MATLAB models provided almost equally accurate results for the individual components when using the updated material properties.

Six configurations of the assembled floor were considered. In all cases, the plywood board was fastened to the beams by screws. Three different distances between the screws in the longitudinal direction were considered, and either one single or three lines of screws were used per beam. The panels were all analysed by OMA, and the panel with single lines of screws and the largest distance between the screws was found to have significantly lower eigenfrequencies than the panel with shorter distance between the screws and three lines of screws per beam.

The experimental results for the floor panels were used to validate the FE models of the panels. It was found that the FE models performed poorly when the plywood board was simply merged with the beams within the models. When introducing an artificial soft elastic layer and a model of the screws into the FE models, higher accuracy could be obtained. A further improvement was achieved by using the updated material properties. However, no conclusion could be made whether the exact values extracted for each individual component should be used, or if average values based on all beams or plates should be employed. In any case, the relative error between the eigenfrequencies of the mock-ups and the FE models of the floor panels were about 0–5 %.

It was found that an FE model based on structural finite elements, i.e. beam and shell elements, could not represent the response of the panels with only single lines of screws and the longer distances between the screws. With a direct coupling between the nodes of the beams and those of the plate, the link is too rigid. One idea for future research is to develop a model with a flexible link between the beams and the plate, using the existing OMA results to calibrate the translational and rotational springs of this coupling.

Further, the present analyses all assumed that the material in each beam is homogeneous, and that the material in all layers of the plywood boards is identical and homogeneous within each layer. Obviously, wood is a heterogeneous material with significant variations of the properties from one position to another. This was demonstrated, for example, by the variation in material density between the four beams in this study. Future research on the heterogeneity of timber and plywood, and its impact on the modal properties of floor panels, is proposed. Identification based on the mode shapes, not only the eigenfrequencies, should be performed.

ACKNOWLEDGMENTS

The authors would like to thank Peter Olsen and Jørgen Holm, Aarhus School of Engineering, Aarhus University, as well as Thomas Kabel, Department of Engineering, Aarhus University, for their involvement in various parts of the research project that was funded by the university.

REFERENCES

[1] M.G. Smith, I. Croy, O. Hammar, M. Ögren, K.P. Waye, Nocturnal vibration and noise from freight trains impacts sleep, Proc. Meet. Acoust. 19 (2013). https://doi.org/10.1121/1.4800407.

[2] T. Münzel, F.P. Schmidt, S. Steven, J. Herzog, A. Daiber, M. Sørensen, Environmental Noise and the Cardiovascular System, J. Am. Coll. Cardiol. 71 (2018) 688–697. https://doi.org/10.1016/j.jacc.2017.12.015.

[3] E. Pedersen, City dweller responses to multiple stressors intruding into their homes: Noise, light, odour, and vibration, Int. J. Environ. Res. Public Health. (2015). https://doi.org/10.3390/ijerph120303246.

[4] P. Persson, C. Frier, L. Pedersen, L.V. Andersen, L. Manuel, Influence of uncertain parameters on modal properties of wood floors, in: A. Zingoni (Ed.), Adv. Eng. Mater. Struct. Syst. Innov. Mech. Appl., CRC Press, Taylor & Francis Group, London, London, 2019.

[5] H.U. Lim, L. Manuel, P. Persson, L.V. Andersen, A surrogate model to describe uncertainties in wood floor modal frequencies, in: A. Zingoni (Ed.), Adv. Eng. Mater. Struct. Syst. Innov. Mech. Appl., CRC Press, Taylor & Francis Group, London, London, 2019.

[6] L. Pedersen, C. Frier, L. Andersen, Flooring-systems and their interaction with usage of the floor, in: Conf. Proc. Soc. Exp. Mech. Ser., 2017. https://doi.org/10.1007/978-3-319-54777-0_25.

[7] C. Frier, L. Pedersen, L.V. Andersen, Non-structural Masses and Their Influence on Floor Natural Frequencies, in: S. Pakzad (Ed.), Dyn. Civ. Struct. Vol. 2. Conf. Proc. Soc. Exp. Mech. Ser., Springer, Cham, 2019: pp. 59–65. https://doi.org/10.1007/978-3-319-74421-6_9.

[8] C. Frier, L. Pedersen, L.V. Andersen, Floor Vibrations and Elevated Non-structural Masses, in: 2020: pp. 103–110. https://doi.org/10.1007/978-3-030-12115-0_13.

[9] L.V. Andersen, C. Frier, L. Pedersen, P. Persson, Influence of Furniture on the Modal Properties of Wooden Floors, in: 2020: pp. 197–204. https://doi.org/10.1007/978-3-030-12075-7_22.

[10] L.V. Andersen, C. Frier, L. Pedersen, Probabilistic Analysis of Modal Properties for Floor Systems with Uncertain Support Conditions, in: S. Pakzad (Ed.), Dyn. Civ. Struct. Vol. 2. Conf. Proc. Soc. Exp. Mech. Ser., Springer, Cham, 2019: pp. 67–75. https://doi.org/10.1007/978-3-319-74421-6_10.

[11] L.V. Andersen, P.H. Kirkegaard, Vibrations in a multi-storey lightweight building structure: Influence of connections and nonstructural mass, in: Res. Appl. Struct. Eng. Mech. Comput. – Proc. 5th Int. Conf. Struct. Eng. Mech. Comput. SEMC 2013, 2013.

[12] J. Negreira, A. Sjöström, D. Bard, Low frequency vibroacoustic investigation of wooden T-junctions, Appl. Acoust. 105 (2016) 1–12. https://doi.org/10.1016/j.apacoust.2015.11.016.

[13] G. Kouroussis, L. Ben Fekih, T. Descamps, Assessment of timber element mechanical properties using experimental modal analysis, Constr. Build. Mater. (2017). https://doi.org/10.1016/j.conbuildmat.2016.12.081.

[14] O. Flodén, K. Persson, G. Sandberg, A multi-level model correlation approach for low-frequency vibration transmission in wood structures, Eng. Struct. 157 (2018) 27–41. https://doi.org/10.1016/J.ENGSTRUCT.2017.11.062.

[15] P. Persson, O. Flodén, Towards uncertainty quantification of vibrations in wood floors, in: Proc. 25th Int. Congr. Sound Vib., Hiroshima, Japan, 2018: pp. 1–8.

[16] R. Brincker, C.E. Ventura, Introduction to Operational Modal Analysis, 2015. https://doi.org/10.1002/9781118535141.

[17] E. Orlowitz, A. Brandt, Comparison of experimental and operational modal analysis on a laboratory test plate, Meas. J. Int. Meas. Confed. (2017). https://doi.org/10.1016/j.measurement.2017.02.001.

[18] C. Gerrand, The equivalent orthotropic elastic properties of plywood, Wood Sci. Technol. 21 (1987) 335–348. https://doi.org/10.1007/BF00380201.

[19] K.A. Dickow, Prediction of Noise Transmission in Lightweight Building Structures, Department of Civil Engineering, Aalborg University, 2014.

[20] SignalExpress 2015 version 15.0.0, National Instruments, Austin, Texas, USA, 2015.

[21] DAQ Assistant version 7.0.0, National Instruments, Austin, Texas, USA, 2019.

[22] ARTeMIS Modal Pro version 6.0.2.2, Structural Vibraton Solutions, Aalborg, Denmark, 2019.

[23] MATLAB version 9.6.0.1072779 (R2019a), Mathworks, Natick, Massachusetts, USA, 2019.

[24] FEMtools version 4.1.0, Dynamic Design Solutions, Leuven, Belgium, 2019.

[25] K.A. Dickow, P.H. Kirkegaard, L.V. Andersen, An evaluation of test and physical uncertainty of measuring vibration in wooden junctions, in: Int. Conf. Noise Vib. Eng. 2012, ISMA 2012, Incl. USD 2012 Int. Conf. Uncertain. Struct. Dyn., 2012.

[26] R.J. Allemang, The modal assurance criterion - Twenty years of use and abuse, Sound Vib. 37 (2003) 14–23.

[27] T. Lauwagie, E. Dascotte, Layered Material Identification using Multi-Model Updating, in: Proc. 3rd Int. Conf. Struct. Dyn. Model. – Test, Anal. Correl. Valid. – Madeira Island, Port., 2002.

[28] T. Lauwagie, Vibration-based methods for the identification of the elastic properties of layered materials, KU Leuven, 2005.